UNIVERSITY OF CALIFORNIA
RIVERSIDE

Reversible Synthesis Graphene Oxide Through Controllable Chemical Potential via Back-Gate Bias: Mechanism and Application

A Thesis submitted in partial satisfaction
of the requirements for the degree of

Master of Science

in

Chemical and Environmental Engineering

by

Chun-Te Kuo

June 2015

Thesis Committee:

Dr. Ming Liu, Chairperson
Dr. Juchen Guo
Dr. Bryan Wong

The Thesis of Chun-Te Kuo is approved by:

_____

_____

_____

Committee Chairperson

University of California, Riverside

Acknowledgements

I would like to thank Dr. Ming Liu and Dr. Ruoxue Yan for introducing me to scientific research, for continuously supervising my work and guiding it by helpful advices and discussion.

Many thanks for my wife Pin-Shan for the loving supporting.

Dedication

To my lovely family.

ABSTRACT OF THE THESIS

Reversible Synthesis Graphene Oxide Through Controllable Chemical Potential via Back-Gate Bias: Mechanism and Application

by

Chun-Te Kuo

Master of Science, Graduate Program in Chemical and Environmental Engineering
University of California, Riverside, June 2015
Dr. Ming Liu, Chairperson

Graphene is a single layer of carbon atoms densely packed in a two-dimensional (2D) sp^2 -bonded carbon hexagonal lattice and is considered as an essential structure element for a variety of carbon materials. Graphene oxide (GO) is chemically modified graphene containing oxygen functional groups and has conventionally served as a precursor for graphene synthesis. Recently GO has received much more attention by scientists for its unique chemical and electrical properties. For example, when covalently functionalized with oxygen-containing functional groups both on the basal plane and at the edges, GO has an assortment of sp2- and sp3-hybridized carbon atoms. Hence, the availability of numerous types of oxygen-containing functional groups lets GO react with a great range of organic and inorganic materials in covalent,

non-covalent or ionic methods so that functional hybrids and composites with remarkable properties can be likely synthesized. Chemically treating a variety of size, shape and relative fractions of sp2-hybridized domains of GO becomes a powerful approach for application-purposed design and preparation of functionalized carbon materials for its optoelectronic characteristics[1-3]. Furthermore, compared with pristine graphene, GO is fluorescent over a broad range of wavelengths, because of its mixed electronic structures[3-5]. The objectives of this work is to design of a graphene-based device with reversibly controllable graphene/graphene oxide ratio through chemical and electrical approaches.

Table of Contents

List of Figures

List of Tables

1. Introduction

1.1 Graphene Background

Graphene as a two-dimensional (2D) crystal not only hold many remarkable properties but also is the basic building material of many forms of sp^2 bonded carbon. It can be wrapped into fullerenes molecules where carbon atoms are arranged in spherical mode by introduction of pentagons as positive curvature defects. These fullerenes have discrete energy states and can be considered as zero dimensional (0D)[6] graphitic structures. Graphene can be rolled along a particular direction and the carbon bonds can be reconnected to generate 1-dimensional (1D) nanostructures called as carbon nanotubes (CNTs)[7] consisting of only hexagons of carbon atoms. The three-dimensional (3D) structure, graphite, formed by stacking graphene sheet attached by van der Wall forces. Different allotropes of carbon are shown in Figure 1.1[8].

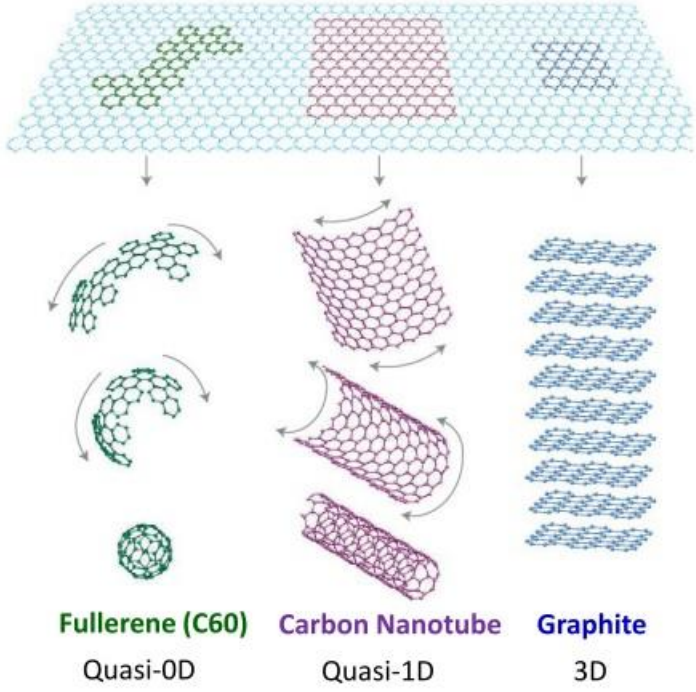

Figure 1.1 Graphene as a building material of various forms of sp^2 carbon materials such as fullerene, carbon nanotube, and graphite[8]

Since the discovery of graphene in 2004, graphene has been claimed as the savior of Moore's law. Moore's law states that the number of transistors in integrated circuits doubles every two years[9].

1.2 Graphene Band structure

Many distinctive physical and chemical properties of graphene are closely related to its 2D crystalline structure and the resulting electronic band structure. Graphene is made out of carbon atoms arranged in hexagonal structure, as shown in Fig. 1.2. Each carbon atom with C-C bonding length (a = 1.42Å) apart from its nearest neighbors in a plane and shares a sp^2 hybridized σ bond with them. The forth p_z orbital (in z direction) consisting of single electron which is perpendicular to the graphene carbon atom plane, and is in charge for conductivity of graphene. These p_z electrons from each carbon atom hybridize to form π and π* bands which make graphene have many special electronic properties.[10,11] the unit cell and corresponding reciprocal lattice of graphene is shown in Figure 1.2. The basis of unit cell consists of two triangular lattice shown by A and B type atoms. The lattice vectors and reciprocal lattice vectors are given by Equation 1.1 and 1.2. The graphene crystalline structure can be seen as a triangular lattice with a basis of two atoms per unit cell. The lattice vectors are given by Equation 1.1

$$a_1 = \frac{a}{2}(3, \sqrt{3}), \qquad a_2 = \frac{a}{2}(3, -\sqrt{3}) \qquad (1.1)$$

Where a=1.42 Å is the carbon-carbon distance. The reciprocal-lattice vectors are given by Equation 1.2.

$$b_1 = \frac{2\pi}{3a}(1, \sqrt{3}), \qquad b_2 = \frac{2\pi}{3a}(1, -\sqrt{3}) \tag{1.2}$$

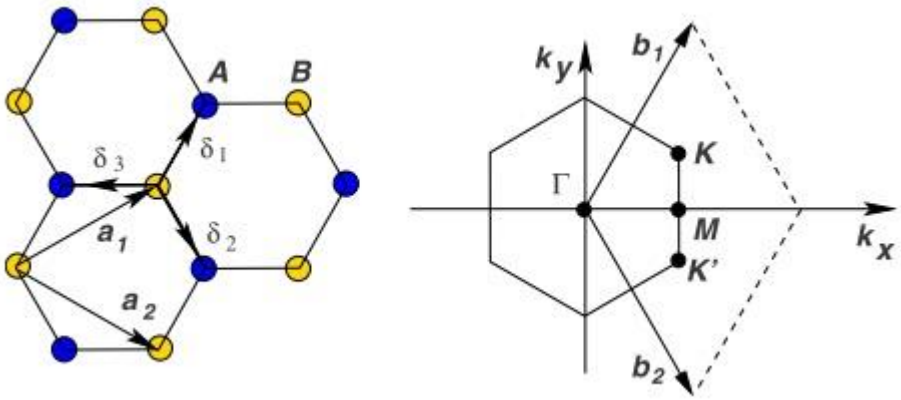

Figure 1.2 Honeycomb lattice and its Brillouin zone. (a) Lift: lattice structure of graphene, made out of two interpenetrating triangular lattices a_1 and a_2 are the lattice unit vectors, and δ_i, i=1,2,3 are the nearest-neighbor vectors. (b) Right: corresponding Brillouin zone. The Dirac cones are located at the K and K' points.[10]

In order to achieve graphene band structure, we consider the interaction of carbon atoms to first nearest and second nearest neighboring carbon atoms. Each carbon atom has three nearest and six nearest neighbors shown in Figure 1.2(a). The hopping of p_z electron is potential for nearest site (A to B) or second nearest site (A to A). The interaction energy is given by t ~ 2.8 eV for A to B atoms hopping and t' ~ 0.1 eV for A to A atoms hopping. The dispersion relation is given by Equation 1.3.

$$E(k) = \pm t\sqrt{3 + 2\cos(\sqrt{3}\,kya) + 4\cos(\tfrac{\sqrt{3}}{2}kya)\cos(\tfrac{3}{2}kxa)} \quad (1.3)$$

where k is reciprocal lattice vector.[10] The positive term in Equation 1.3 corresponds to conduction band and negative is for valence bands as plotted in Figure 1.3[10,12]. The Dirac point is the crossing point of the linear energy dispersion curves of positive term and negative term which is the low energy points in reciprocal lattice space. Conduction band and valence band meet each other at these Dirac points at 6 places[12] at the corner of graphene Brillouin zone (BZ) shown in Figure 1.4, referred as K and K' points. Both K and K' positions in momentum space are given by Equation 1.4

$$K=\left(\frac{2\pi}{3a}, \frac{2\pi}{3\sqrt{3}a}\right) \qquad K'=\left(\frac{2\pi}{3a}, -\frac{2\pi}{3\sqrt{3}a}\right) \tag{1.4}$$

The three nearest-neighbor vectors in real space are given by Equation 1.5

$$\delta_1 = \frac{a}{2}(1, \sqrt{3}),\ \delta_2=\frac{a}{2}(1,-\sqrt{3}),\ \delta_3=-a(1,0) \tag{1.5}$$

While the six second-nearest neighbors are located at

$$\delta_1' = \pm a_1,\ \delta_2'=\pm a_1,\ \delta_3'=\pm (a_2-a_1) \tag{1.6}$$

The dispersion relation at K and K' points and within ±1 eV vicinity of the Dirac point is given by the following linear relationship.

$$E(k) = \pm h v_F |k| = \pm v_F \sqrt{k_x^2+k_y^2} \tag{1.7}$$

Where v_F is Fermi velocity given by

$$v_F = \frac{3at}{2h} \approx 0.9 \times 10^6 \text{ m/s} \tag{1.8}$$

This linear dispersion relationship described by Equation 1.7 at low energy makes electrons and holes both move with Fermi velocity. Thus, charge particles in graphene close to Dirac point is called as Dirac fermions.

This is especially different at low energy level compared with most of the bulk semiconductors which have parabolic dispersion relationship. The linear dispersion relationship of graphene is also in charge for electronic properties of vanishing density of states (DOS) at Dirac points. The DOS in graphene is given by[13,14]

$$\text{DOS} = \frac{E}{2\pi h^2 v_F^2} \qquad (1.9)$$

The zero band gap state of graphene at Dirac point which has no charge carriers also called as intrinsic state.

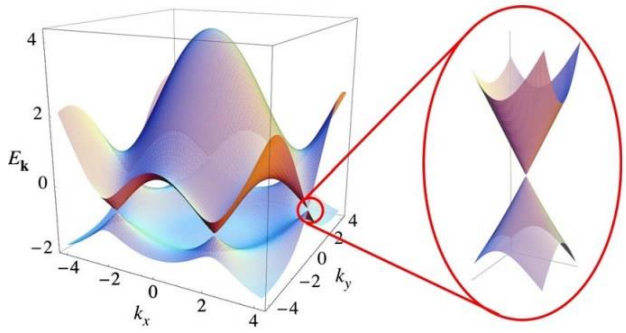

Figure 1.3 Electronic dispersion in monolayer graphene in the units of t = 2.7 eV. The upper band is conduction band and lower one is valence band. The zoom in diagram on the right shows linear relationship close to Dirac point where conduction band and valance band meet each other.

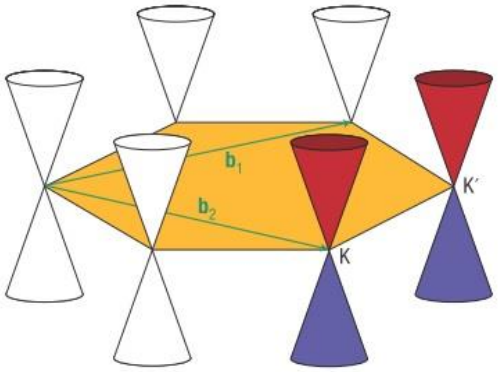

Figure 1.4 The low-energy electronic structure of graphene. The conduction band and the valence band meet at six points which known as Dirac points at the corners of the Brillouin zone in momentum space.

1.3 Graphene Electrical Properties

1.3.1 Electric field effect in graphene

Electric field effect happens when vertical electric field, either top-gate or back gate, applied to graphene plane can induce electrons or holes which depending upon the direction of the electric field. The Fermi level (E_F) can be lifted up in conduction band inducing electrons, and can be lowered down in valance band inducing holes which results in ambipolar of graphene channel shown in Figure. 1.5.[8] The Fermi level and Density of Energy of intrinsic graphene should be zero without externally applied electric field according to Equation 1.9. However, there always are finite charges present because of impurities trapped at graphene and substrate interface. For this reason, graphene based field effect transistor cannot be turn on or off by the threshold voltage. The current on/off ratio in graphene based FETs locates in the range ~ 10 thus make them inappropriate for switching device application in spite of their high mobility values.

1.3.2 Electronic mobility of graphene

The major scattering mechanism in graphene are Coulomb scattering[15], phonon scattering[16] and short-range scattering[17] primarily as a result of defects as vacancies and cracks in graphene. The mobility is mostly dependent upon the quality of

graphene and underlying substrates based on those scattering mechanism operating in graphene. For example, at room temperature surface polar phonons and defects dominate scattering mechanism for graphene on SiO_2 substrate, while at lower temperature phonons turn out to be more important. The typical mobility values[18] of high-quality graphene on SiO_2 higher than 10000 $cm^2V^{-1}s^{-1}$ which is much higher than traditional semiconductors. Furthermore, the electron mobility in suspended graphene has been reported as high as 200,000 $cm^2V^{-1}s^{-1}$ for charge density below $5\times10^9cm^{-2}$ at low temperature.[19,20] However, the electron mobility of supported graphene on SiO_2 will have a maximum limit of 40,000 $cm^2V^{-1}s^{-1}$ at room temperature as a result of optical phonon scattering of the substrate.

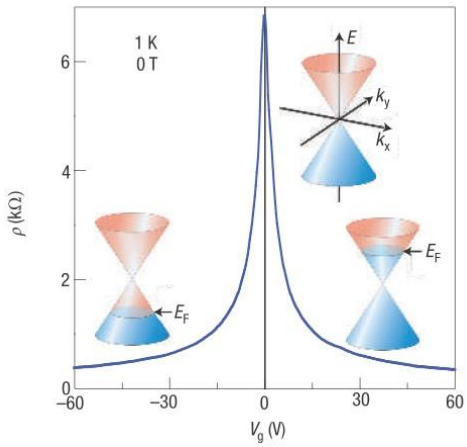

Figure 1.5 Ambipolar electric field effect of a single-layer pristine graphene[8]. The Fermi level E_F is located at Dirac point with Vg= 0V. The insets show its conical low-energy spectrum E(k), indicating changes in the position of the Fermi energy E_F while changing gate voltage V_g. Positive V_g induce electrons and negative V_g induce holes.

1.3.3 Graphene Chemical Properties

Graphene, as a 2D material with very high surface to volume ratio, coupled with delocalized π electrons as an effect of sp^2 hybridization in C-C bond causes it to be a great sensing material shown in Figure 1.6. The 2D material property of graphene film makes it enabling absorb or react with analyte molecules very efficiently and generate the maximum change in its chemical and electrical properties. Additional, graphene surface could be change or modify via adsorption reaction to a large variety of analytes with its delocalized π electrons. The low-frequency noise characteristics of graphene have also been very notable in the range of 10^{-9}~10^{-7} Hz^{-1} compared with carbon nanotubes (CNTs).[21] Generally, graphene have been demonstrated with very low 1/f and thermal noise.[22]These outstanding material properties have led to the protest of graphene based sensors that are able to detecting single analyte molecule.[23]

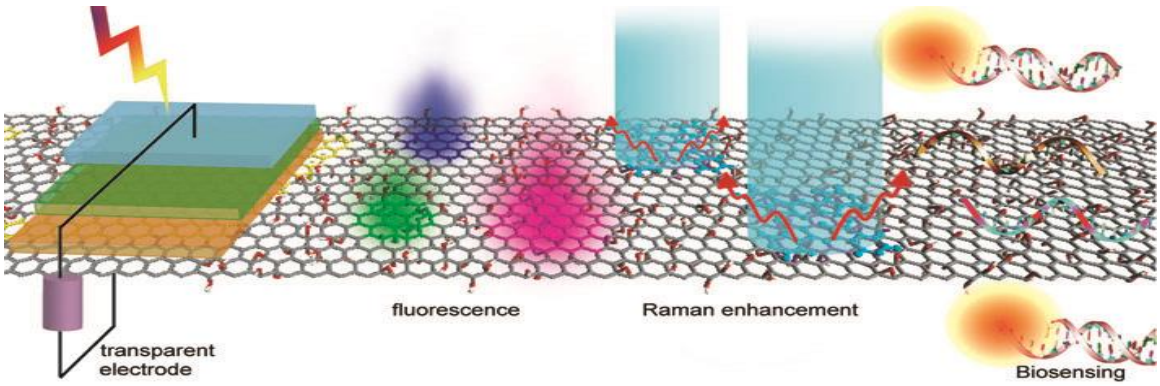

Figure 1.6 Various physical and chemical applications of graphene oxide.[2]

1.4 Applications for graphene

As a combination of various remarkable properties, graphene enables its application in variety of diverse areas such as chemical sensors, hydrogen storage, mechanical sensors, NEMS devices, laser material, transparent electrodes, wiring material, high speed transistors, spin devices, single electron transistor, semiconductor memory, solar cells, separation membrane. Figure 1.7 shows major applications[24] of graphene which have already been demonstrated utilizing different properties of graphene. Figure 1.8 shows a chart for applications that graphene companies were targeting in 2011. This chart was organized from a broad survey of graphene companies and clearly highlights the versatility of graphene.

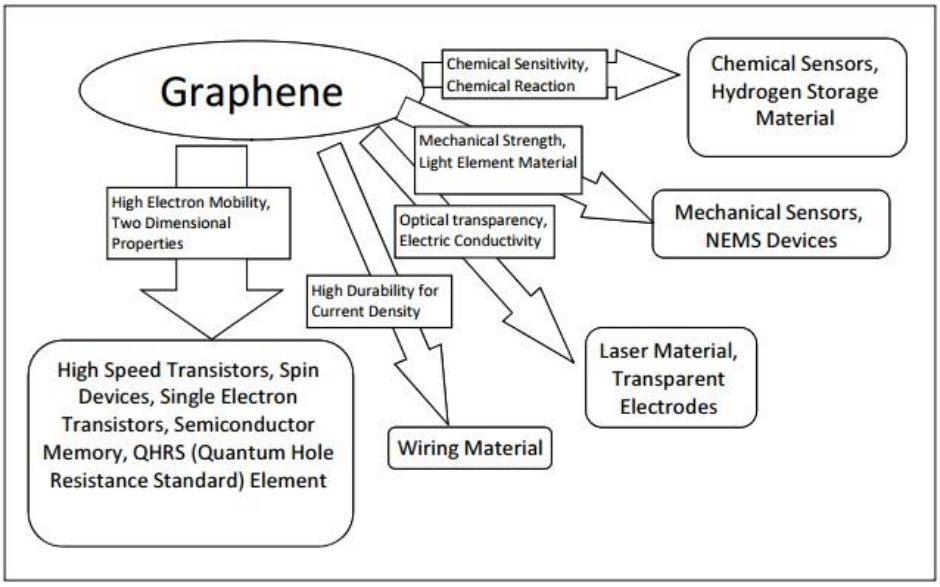

Figure 1.7 Distinctive Properties of Graphene and Possible Application Fields.[24]

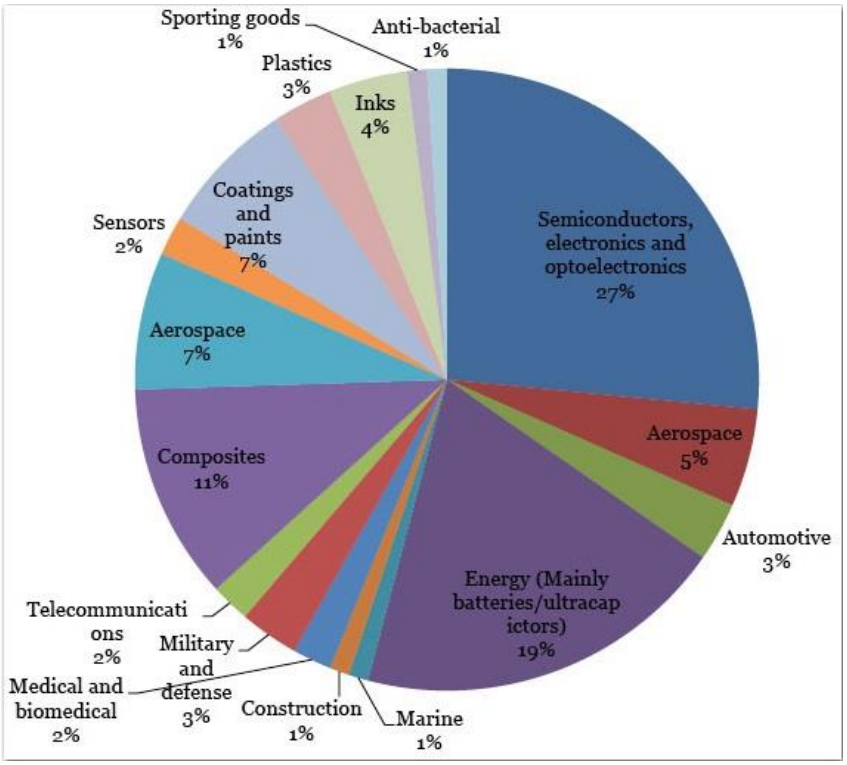

Figure 1.8 Applications chart for graphene companies.

2. Research Motivation and Objectives

2.1 Research Motivation

. Graphene is a single layer of carbon atoms densely packed in a two-dimensional (2D) sp^2 -bonded carbon hexagonal lattice and is considered as an essential structure element for a variety of carbon materials. Graphene has recently attracted considerable attention owing to its remarkable electronic and structural properties and for use in possible applications in many emerging areas such as graphene-based electronic and optical devices[8,25]. The charge carriers in graphene behave like massless Dirac fermions[26], with ballistic transport between widely spaced scattering centers[27], and therefore it is considered as a promising electrical material for the post-silicon era. However, the linear electronic band structure in graphene means the lack of a bandgap near the Dirac point, which is critical for semiconductor materials[28]. One approach to create a bandgap is to convert graphene into GO by using a chemical solution treatment. As a result, graphene oxide (GO) is a tunable platform on both electrically conductive[29] and chemically active bonding spots which allow it to be a prospective candidate as a sensing material[30] and also a photodetector[31-34].

2.2 Research Objectives

We propose a new approach to opening and tuning band gap in graphene by controlling the reversible oxidation reaction on a back-gated graphene film immerged in sulfuric acid, as shown in Figure 2.1.

First, we put a droplet of sulfuric acid (<1 mL) on top of graphene film and then apply different back-gate voltages to change the chemical potential of graphene which further induce the oxidation reaction. Forming a simple parallel capacitor between graphene film and silicon substrate, negative bias voltage applied on the substrate will induce positive charge accumulation on graphene. Groups with negative charges in the solution, such as bisulfate anion (HSO_4^{-1}) and sulfate anion (SO_4^{-2}), will be attracted to the positive charged graphene surface and form a Stem layer in the vicinity. With various back-gated voltages and reaction times, the anions accumulated in the Stem layer will break sp^2-bonds to form sp^3-bonds and start to convert graphene into GO. Furthermore, with this synthesis method, we can precisely control the reversible reaction and achieve appropriate graphene/graphene oxide ratios for various applications to utilize the unique electrical, optical and chemical properties of GO. The product may cover a broad range of electrical properties, ranging from highly conductive zero-overlap semimetal, sub-eV bandgap semiconductor to full

insulator.

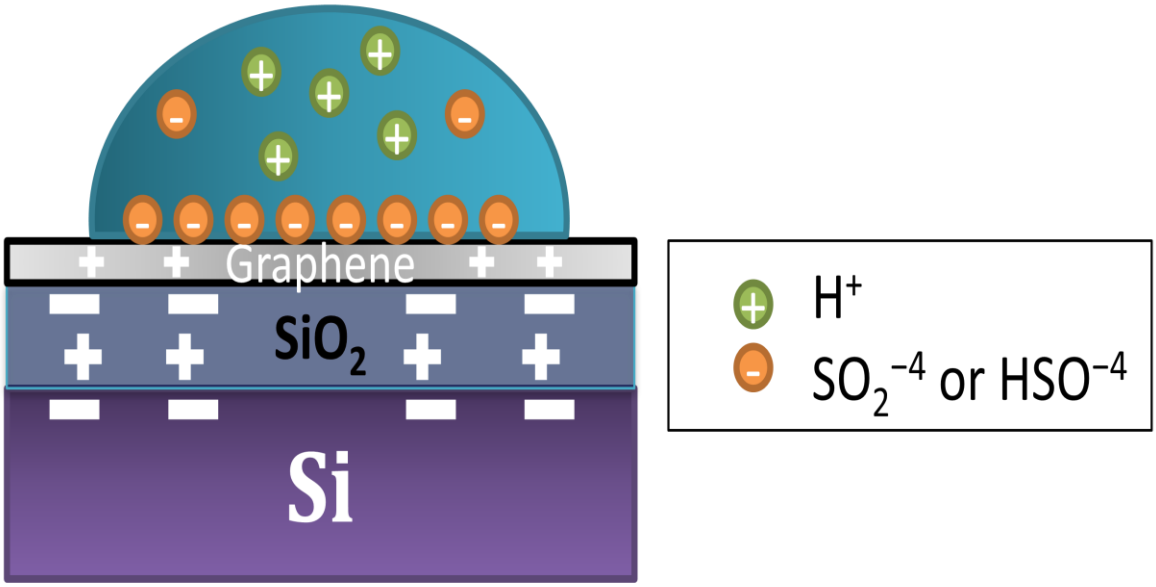

Figure 2.1 Diagram of device with sulfuric droplet on top of graphene when negative bias voltage applied on the substrate.

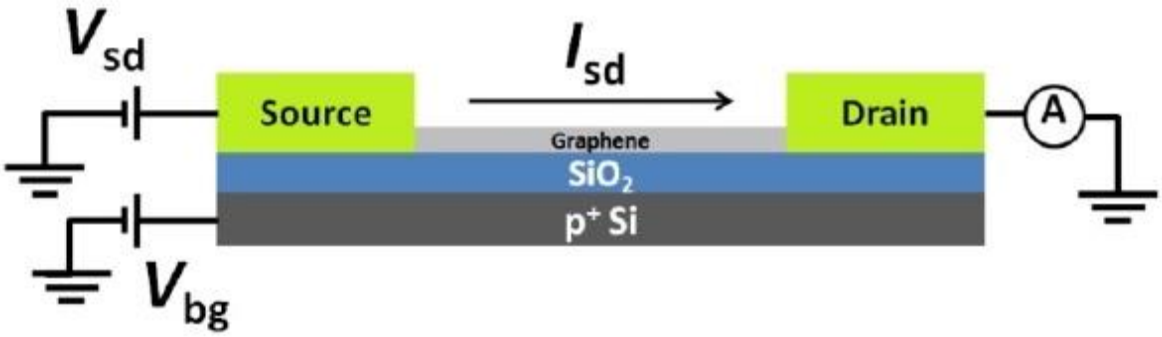

Figure 2.2 Schematic of a graphene field effect transistor.[4]

3. Material and Methods

3.1 Graphene synthesis and transfer

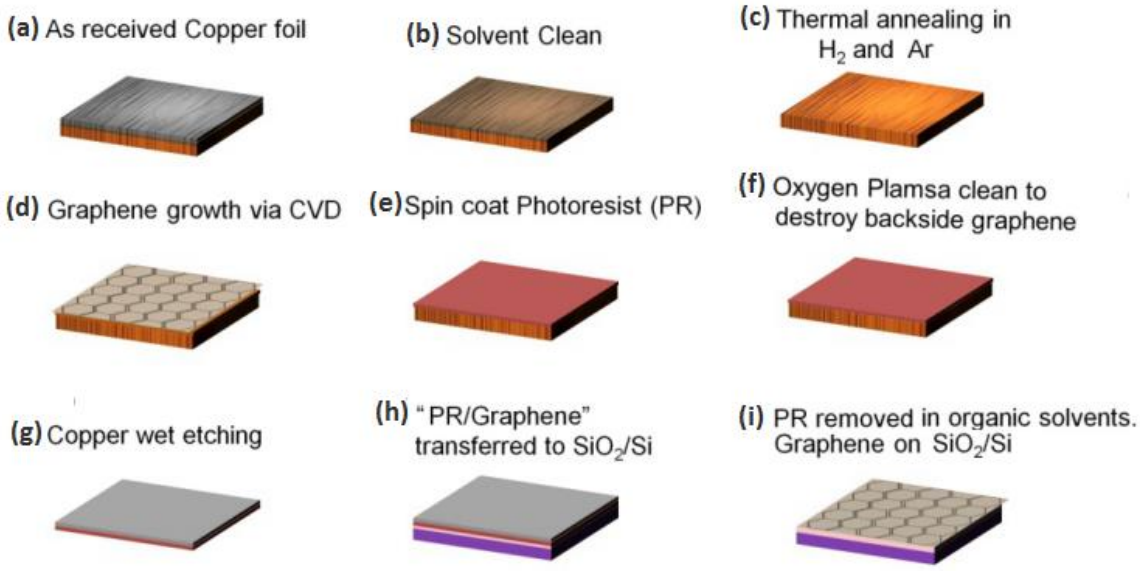

Figure 3.1 Graphene synthesis and transfer process to SiO_2/Si.

3.1.1 Solvent cleaning

The copper foil is 25um thick, 99.8% pure from Sigma-Aldrich. The commercial copper foil may covered by a thin film of organic compounds that may cause the deposition of amorphous carbon at growth process[35], so solvent cleaning process is used to remove them. The solvent cleaning recipe is summarized in Table 1. Firstly, put copper foil immersed into acetic acid to remove native oxide layer and followed by acetone. Acetone is used to remove rest organic compounds

but it also leaves its own residue due to its extremely rapid evaporation rate so isopropyl alcohol is utilized as solvent to remove rest acetone. Finally, foil is placed in De-ionized (DI) water bath to remove remaining organic solvents. After nitrogen gas dry, foil is pressed between two clean quartz slides to keep it as flat as possible.

Table 3-1 Solvent cleaning process.

Acetic acid	Acetone	Isopropyl Alcohol	De-ionized (DI) water
10 min	10 min	10 min	10 min

3.1.2 Thermal annealing

As-received copper foil covered by thin layer of native copper oxide, which is highly inappropriate for graphene growth[36]. Even Acetic acid be used to remove native oxide layer[37] but it makes the surface with high roughness which is also not desirable[38]. Thermal annealing for copper foil is performed in Ar and H_2 at 1030° C. There are two advantages of thermal annealing: (1) remove native copper oxide layer by H_2 reduction[36,39] and (2) increase the grain size of polycrystalline copper foil since as-received copper foil has much smaller grain size with large number of grain boundaries. Graphene mostly prefer to grow on grain boundaries first as compared to smooth copper surface, which eventually leads to double-layer or

multilayer graphene on those regions[40,41]. By using thermal annealing increase grain size of copper surface[36] which reduce the grain boundaries effect during graphene growth process. First, cleaned Cu foil put in a 1 in. quartz tube furnace and heated up to 1030℃ for annealing under Ar flow of 200sccm and H2 flow of 150sccm at 3.60Torr. After reaching the annealing temperature, flow rate of gases were left unchanged and annealing was performed for 2 hours. Argon acts as the carrier gas and H2 is used to reduce the Cu foil. Recipe of thermal annealing is summarized in Table 2.

Table 3-2 Recipe of thermal annealing for copper foil.

Step	Processing Step	Temperature(℃)	Processing gas	Period Time (min)
1	Fast Ramp up	20 to 800	H_2(150 sccm), Ar(200 sccm)	20
2	Slow Ramp up	800 to 1030	H_2(150 sccm), Ar(200 sccm)	20
3	Hold	1030	H_2(150 sccm), Ar(200 sccm)	120

3.1.3 Chemical vapor deposition

For synthesis of single-, double- and multi-layer graphene film, we use a low pressure chemical vapor deposition (CVD) method with polycrystalline copper foils as catalyst in a self-designed hot wall furnace[42,43]. First, We prepare a catalyst substrate by cutting Cu foil (99.8 %, 25 μm thick, Sigma-Aldrich) into 3x6 cm2 rectangle pieces and clean them in acetic acid, acetone, isopropyl alcohol one after another at 10 minute intervals to remove the oxide layer and organic residuals. Subsequently, cleaned Cu foil was then put in a 1 in. quartz tube furnace and heated up to 1030℃ for annealing under Ar flow of 200sccm and H_2 flow of 150sccm at 3.60Torr. Argon acts as the carrier gas and H_2 is used to reduce the Cu foil. After annealing for 2 hours, a mixture of Ar (200sccm)/H_2 (150sccm)/CH_4 (200sccm) gases was introduced into the CVD system to initiate the graphene synthesis on copper foil substrate for 20 min. Finally, after a continuous graphene layer was formed on Cu foil, the system was fast cooled down to room temperature with presence of Ar/H_2/CH_4 mixture gas at 50℃/min of cooling rate. The schematic of the setup and temperature vs time of single-layer graphene growth plot are shown in Figure 3.2 and Figure 3.3.

Figure 3.2 Graphene chemical vapor deposition setup.

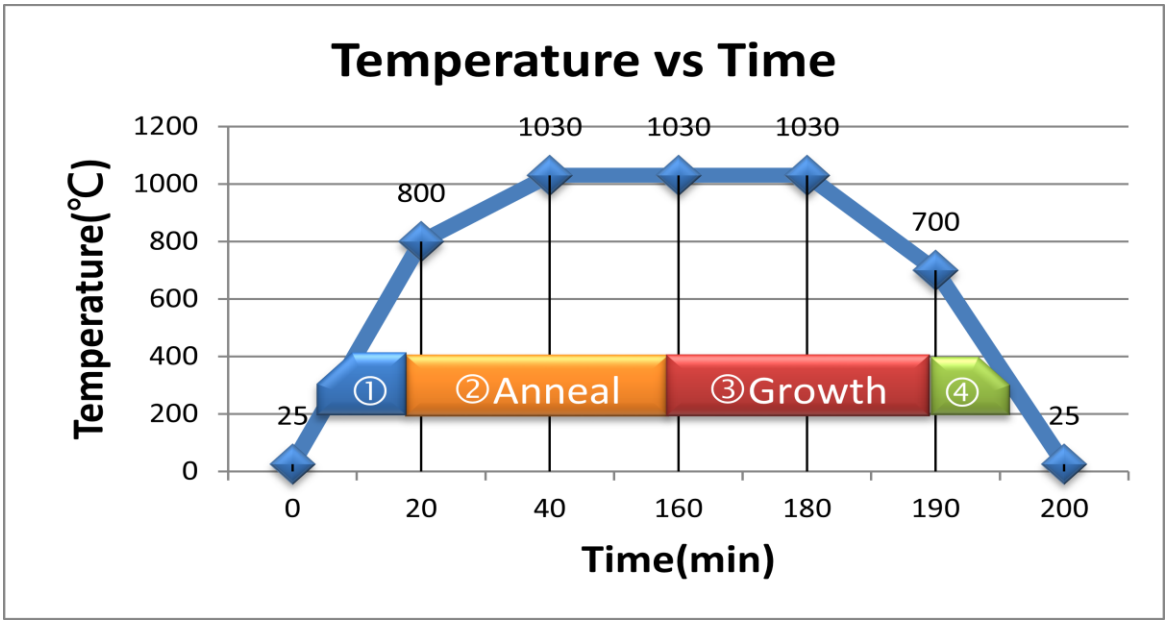

Figure 3.3 Temperature vs. time plot for single-layer graphene synthesis.

Table 3-3 Recipe of single-layer graphene synthesis on copper foil.

Step1	Heating up to 1030℃ with Ar and H_2 in 40 min.
Step2	Annealing at 1030℃ with Ar and H_2 for 2 hours.
Step3	Graphene synthesis by using CH_4 with Ar and H_2 for 20 min.
Step4	Fast cooling to room temperature in 20 min.

3.1.4 Graphene transfer

To facilitate the graphene device, we need to remove the catalytic Cu substrates from graphene and transfer graphene onto target substrates.[42] Graphene was first spin-coated by a thin layer of polymethyl methacrylate (PMMA, 495 A5) at 3000 rpm for 45 second and then baked 10 min at 150 ℃ to evaporate the solvent. Because graphene grows on both sides of the Cu foil, we need to remove graphene which grows on the back side. Firstly, we put the "good" side (the side with better graphene growth) face down on the Si wafer and totally seal all boundaries of Cu foil by tapton tape. The back side graphene is then removed by a Reactive Ion Etcher (RIE) under 50W with O_2 flow of 50sccm for 2 min. After back side graphene is removed, the Cu foil was then etched by 0.4M $FeCl_3$ for 2-3 hours, leaving only the PMMA/graphene film floating on the surface of solution. The films firstly transferred to 0.1M HCl solution to clean the iron ion residual from Cu etchant. After that, graphene films are transferred to deionized (DI) water to clean several times and then transferred onto a SiO_2 substrate. After the water is totally evaporated, substrates are baked on a hot-plate for 10 min at 120 ℃ to increase the adherence between graphene and the SiO_2. In the next step, PMMA was removed by acetone, IPA and DI water leaving a graphene film on top of the SiO_2substrate. The transfer process is then complete.

3.2 Fabrication of Graphene-Based Field Effect Transistor Devices

The first step in the fabrication process is the deposition of the metal electrodes. After the graphene transfer process, the graphene on SiO_2/Si samples was spin-coated with photoresist AZ5214 at 4000 rpm for 45 seconds at a photoresist spin coat station then baked on a hot plate for 3 minutes at 110℃. A Suss MA-6 Mask Aligner was used along with an appropriate alignment mark mask to hard-expose the samples for 2 seconds. After exposure, we re-baked the sample on a hot plate for 3 minute as a reversal bake. After being re-baked, 1 minute flood-exposure was used for reverse imaging exposure. Then, the samples were developed with diluted AZ 351B (1:4=AZ351: DI water) for 30 seconds, rinsed in a short DI bath and dried out by an ultra-high N_2 air gun. During the e-beam metal deposition by using E-beam Evaporation, a 5 nm layer of chrome was deposited first and acted as the sticking layer. 150 nm of gold was then deposited on top of the chrome to create the bulk of the metal electrodes. After electrodes deposition, the samples were placed in acetone or PG remover 1165 for at least 12 hours at 70℃ to remove any photoresist and excess metal. Each sample was cleaned with PG remover, isopropyl alcohol, DI water, and then an ultra-high purity N_2 dry after they were taken out from DI water. The

second step in the process is used to remove all of the graphene from the SiO_2/Si substrate and only leave the graphene nano-ribbons located across the electrode as field effect transistor's channels. The photolithography for this step is identical to the alignment mark procedure by aligning the mask mark with the masker on our first layer fabrication. First, the samples were spin-coated with photoresist AZ5214 at 4000 rpm for 45 seconds and then baked on a hot plate for 3 minutes at 110℃. A Suss MA-6 Mask Aligner was used again with an identical mask with marker for alignment to do first layer fabrication. Then, hard-exposure was applied to the samples for 11 seconds. After exposure, the samples were developed with diluted AZ 400K (1:4=AZ 400K: DI water) for 30 seconds, rinsed in a short DI bath and dried it out by a N_2 gun. Then, we loaded the samples, which were taped onto a Si wafer, into RIE to etch away graphene excluding the area which had been protected by photoresist under O_2 flow of 50 sccm and power of 50W for 2 min. The samples were then placed in acetone or PG remover for at least 2 hours at 70℃ to remove any photoresist. Each sample was cleaned with PG remover, isopropyl alcohol, DI water, and then an ultra-high purity N_2 blow dry after they were taken out from the DI water.

4. Result and Discussion

4.1 Characterization of Graphene samples

4.1.1 Optical microscope

After graphene is synthesized on Cu foil, we put the graphene/Cu substrate on a hot-plate to bake at 180℃ for a quick quality check. After 5 min of baking in air, the area which has no graphene growth will change color resulting from Cu oxidation but the other area covered with continuous graphene will keep the same color as before baking. By using this method, we can immediately determine the area which has graphene growth after CVD synthesis. The optical images of graphene on Cu foil after baking shown in Fig. 4.1 (a)-(f).

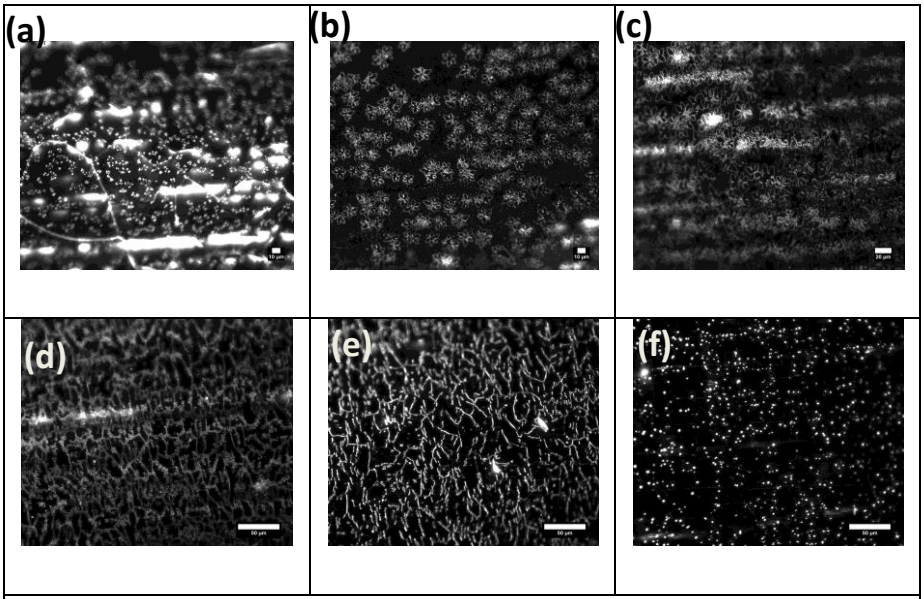

Figure 4.1 (a)-(f). Controlled growth of single-layer graphene by CVD system.

4.1.2 Raman spectroscopy

After we transfer graphene to a SiO_2 substrate, graphene is characterized by Raman spectroscopy. Raman spectroscopy can not only be used to determine the number of layers, but also can identify the quality of graphene samples[44]. The samples were measured by using a confocal laser scanning microscope with laser wavelength of 532 nm and 1800 grooves/mm grating with a 100x objective lens.

A typical Raman spectrum of single-layer graphene is shown in Figure 4.2. The D-peak appears at approximately 1350 cm^{-1} and the G-peak appears at approximately 1580 cm^{-1}. The other Raman peaks are at 1620 cm^{-1} (D' peak), 2680 cm^{-1} (2D peak), and 2947 cm^{-1} (D+G peak). The G peak arises from the stretching of the C-C bond in graphitic materials, and is common to all sp^2 carbon systems. The G peak is highly sensitive to strain effects in a sp^2 system and thus can be used to probe modification on the flat surface of graphene. The D and D' peak is caused by the disordered structure of graphene. The presence of disorder in sp^2 -hybridized carbon systems results in resonance Raman spectra, and thus makes Raman spectroscopy one of the most sensitive techniques to characterize disorder in sp^2 carbon materials. As is shown by a comparison of Figure 4.2 top and bottom figures, there is no D peak in the Raman spectra of graphene with a perfect structure.

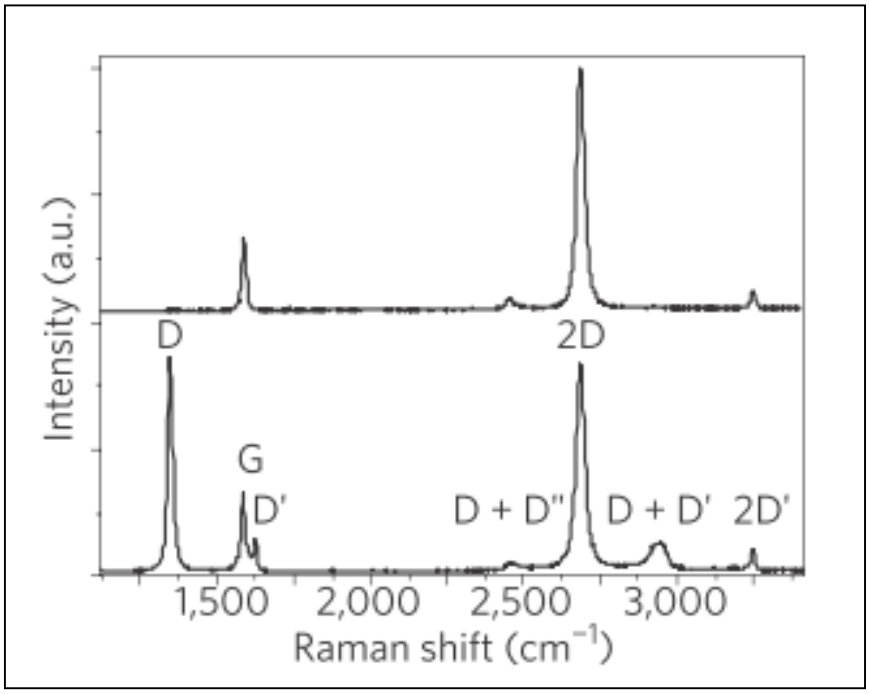

Figure 4.2 Raman spectra of pristine (top) and defected (bottom) graphene. The main peaks are labeled.

The Raman spectras shown in Figure 4.3 and Figure 4.4 are our CVD synthesized graphene samples. The absence of D peak ~ 1350 cm^{-1} indicates the high crystallinity and very low structural defects in graphene. Single-layer graphene samples show I_{2D}/I_G ratio of >1 and a narrow 2D peak with FWHM ~25 cm^{-1}. While bi-layer graphene samples show I_{2D}/I_G ratio ~1 and a broad 2D peak with FWHM ~45 cm^{-1} and for I_{2D}/I_G <1 indicating the existence of multi-layers.[45]

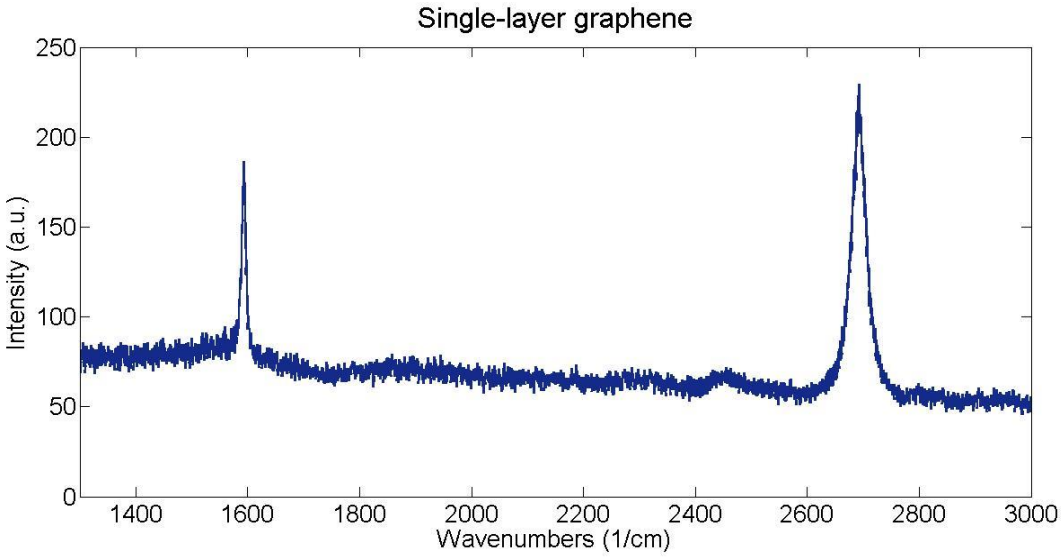

Figure 4.3 Raman spectra of our CVD pristine single-layer graphene.

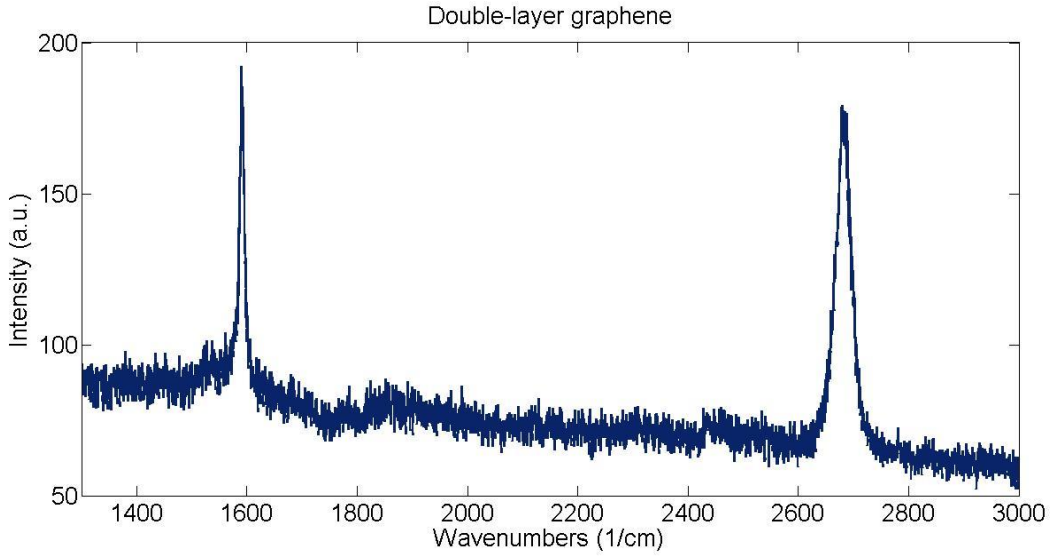

Figure 4.4 Raman spectra of double-layer graphene.

4.2 Graphene based field effect transistor

After Back-gated graphene field-effect transistors (GFETs) were fabricated on Si substrates with 300 nm SiO_2, electronic properties of our CVD transferred graphene was measured with four probe measurement system under ambient conditions. The channel length between source and drain electrodes is 20 μm. The width of the channel is 20 μm. The optical image of the device are shown in Figure 4.5. Back gate bias was applied via the probe to the Si substrate. Drain voltage (V_d) was applied 100 mV with source electrode grounded. The drain current (I_d) was measuring while gate voltage swept from 0 V to 20 V. The Transport property of back-gated graphene field effect transistor (GFET) is depicted in figure 4.6. In Figure 4.6, a minimum conductivity point was measured while back gate voltage around +8V. The back-gate oxide capacitance per area (C_{ox}) for 300 nm SiO_2 is 10 nF-μm^{-2}.

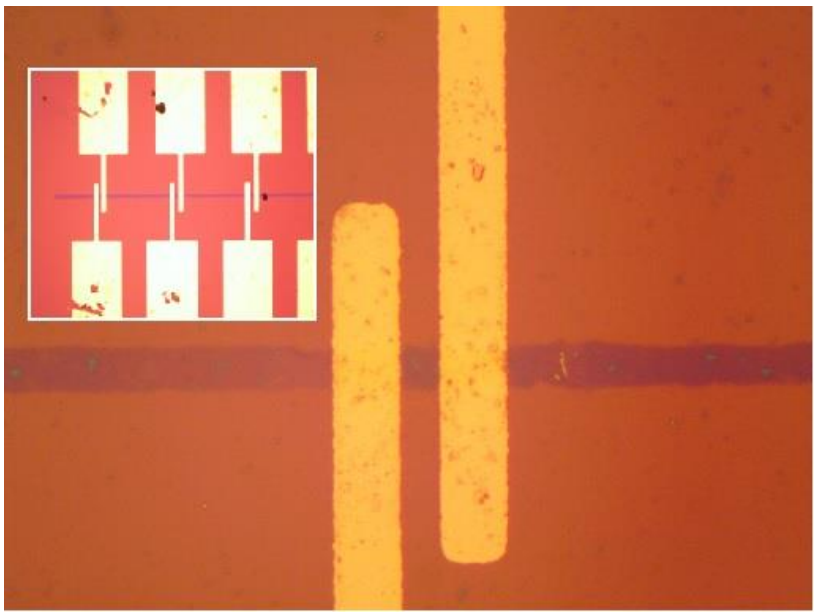

Figure 4.5 Optical images of graphene-based field effect transistor device with various channel length.

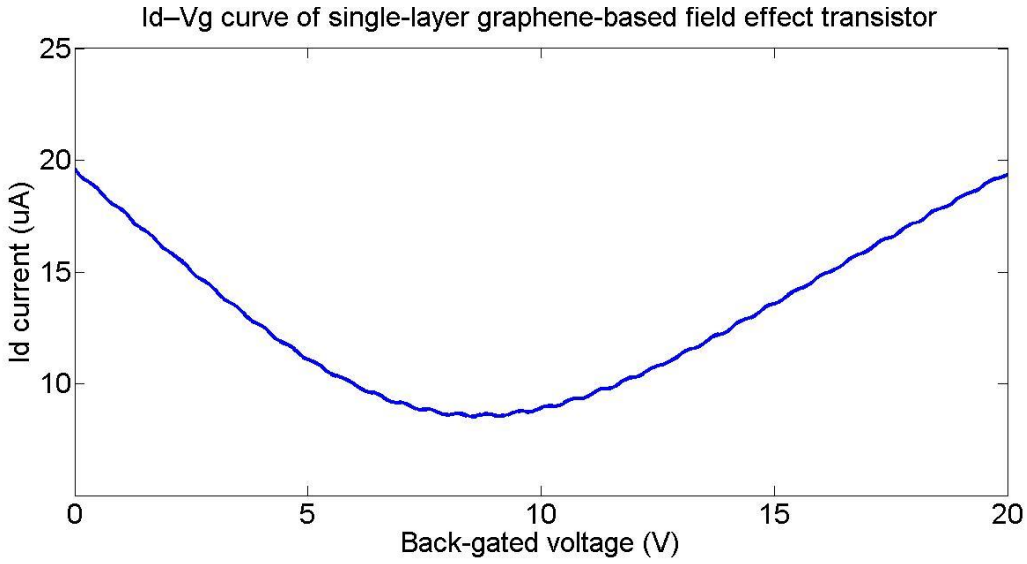

Figure 4.6 Id-Vg curve of single-layer graphene-based field effect transistor.

We can extract the carrier mobility from transfer characteristics. Starting with drift current, we have:

$$\vec{J} = qn\mu\vec{\varepsilon} \quad (4.1)$$

$$\vec{J} = \sigma\vec{\varepsilon} \quad (4.2)$$

Also, carrier concentration can be calculated with Equations 4.3 and 4.4.

$$qn = C_{ox}\left(V_{gs} - V_D\right) \quad (4.3)$$

$$C_{ox} = \frac{\varepsilon_r \varepsilon_0}{d} \quad (4.4)$$

C_{ox} and V_D are geometrical capacitance and gate voltage at minimum conductivity point respectively. Therefore, carrier mobility can be expressed by Equation 4.5.

$$\mu = \frac{\sigma}{qn} = \frac{I_{ds} \times L}{V_{ds} \times W \times C_{ox} \times (V_{gs} - V_D)} \quad (4.5)$$

Mobility extraction is based on trans-conductivity (g_m) which is the slope of linear part of Id-Vg curve of graphene. Accordingly, we replace $\frac{I_{ds}}{(V_{gs} - V_D)}$ with trans-conductivity (g_m), in Equation 4.5.

$$g_m = \frac{I_{ds}}{(V_{gs} - V_D)} \quad (4.6)$$

As a result, mobility is expressed by Equation 4.7.

$$\mu = \frac{g_m}{\frac{W}{L} C_{ox} V_{DS}} \quad (4.7)$$

The extracted trans-conductivity (g_m) is ~1 μA V^{-1} shown in Figure 4.7. The carrier mobility of electrons and holes for this device is calculated by the relation between mobility

(μ) and g_m by Equation 4.7, where V_{DS} is 0.1 V in the measurements. The calculated mobility is about 1400 $cm^2\ V^{-1}\ s^{-1}$, which is comparable to the recent literature.[46-49]

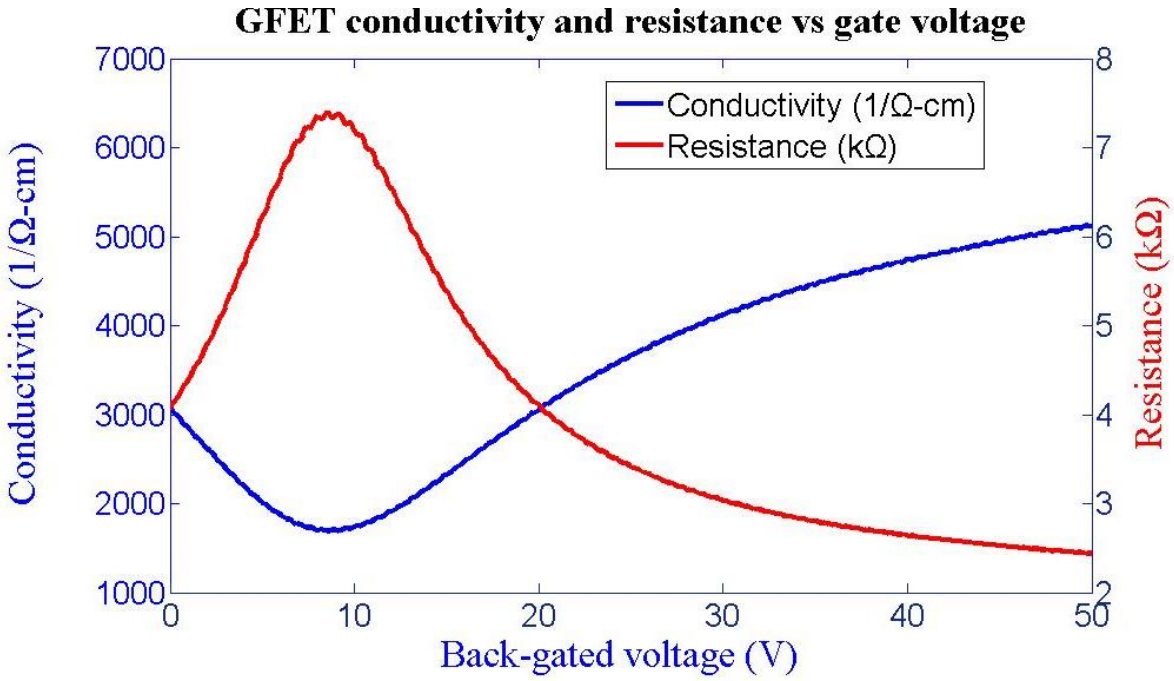

Figure 4.7 GFET conductivity and resistance curve versus back-gate voltage (V_g) from 0V to 50V.

4.3 Effect of back gate bias applied on graphene raman spectroscopy

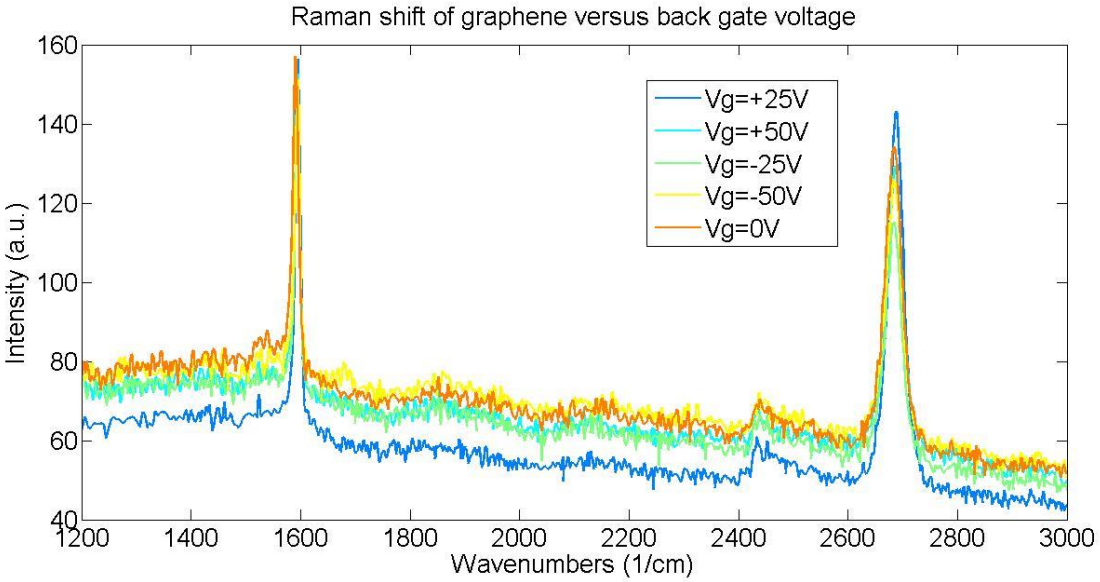

Figure 4.8 Raman shift of graphene versus back gate voltage changed from -50V to +50V.

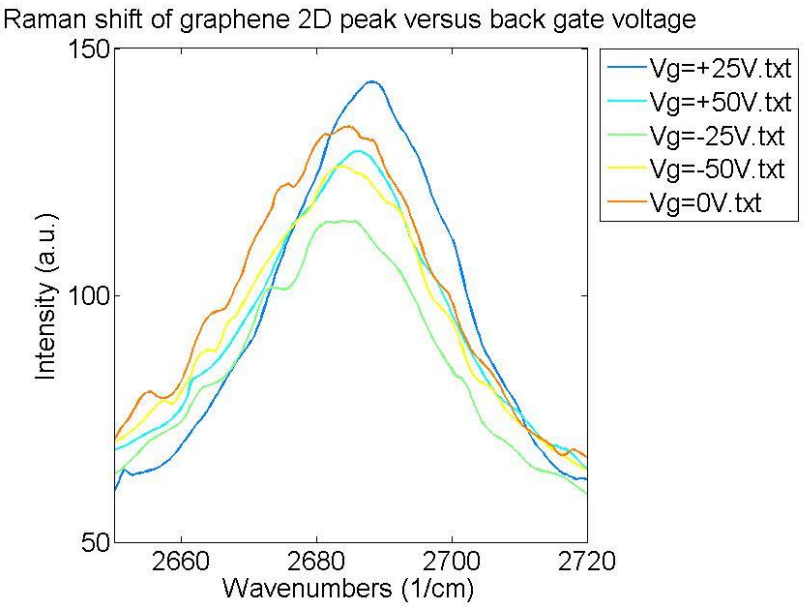

Figure 4.9 Raman shift of graphene 2D peak versus back gate voltage changed from -50V to +50V.

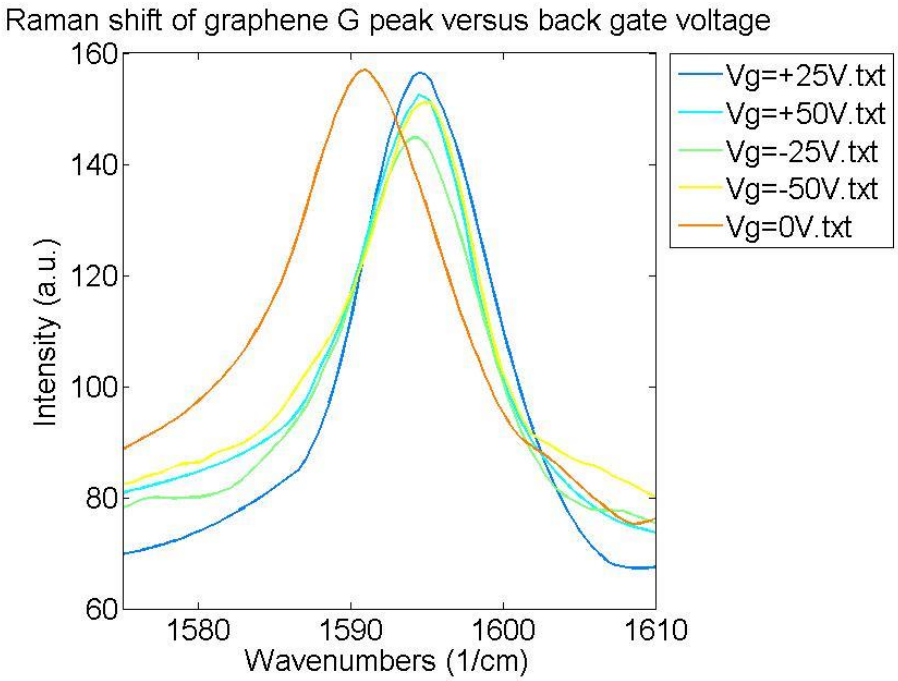

Figure 4.10 Raman shift of graphene G peak versus back gate voltage changed from -50V to +50V.

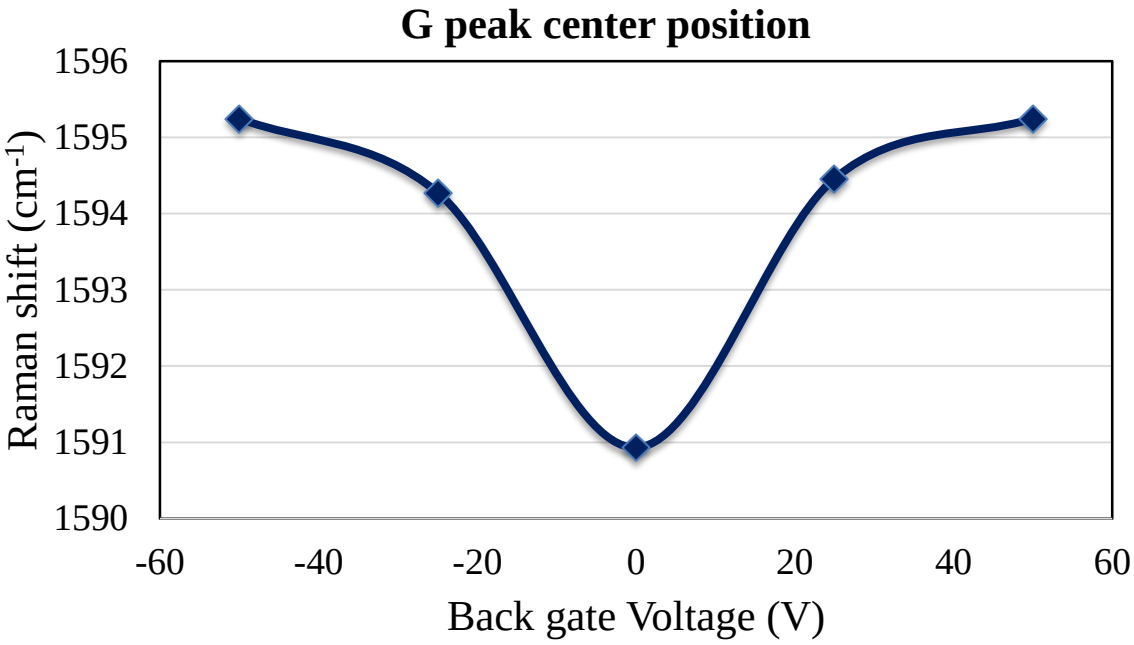

Figure 4.11 Raman shift of graphene G peak center position versus back gate voltage changed from -50V to +50V.

4.4 Effect of sulfuric acid on graphene

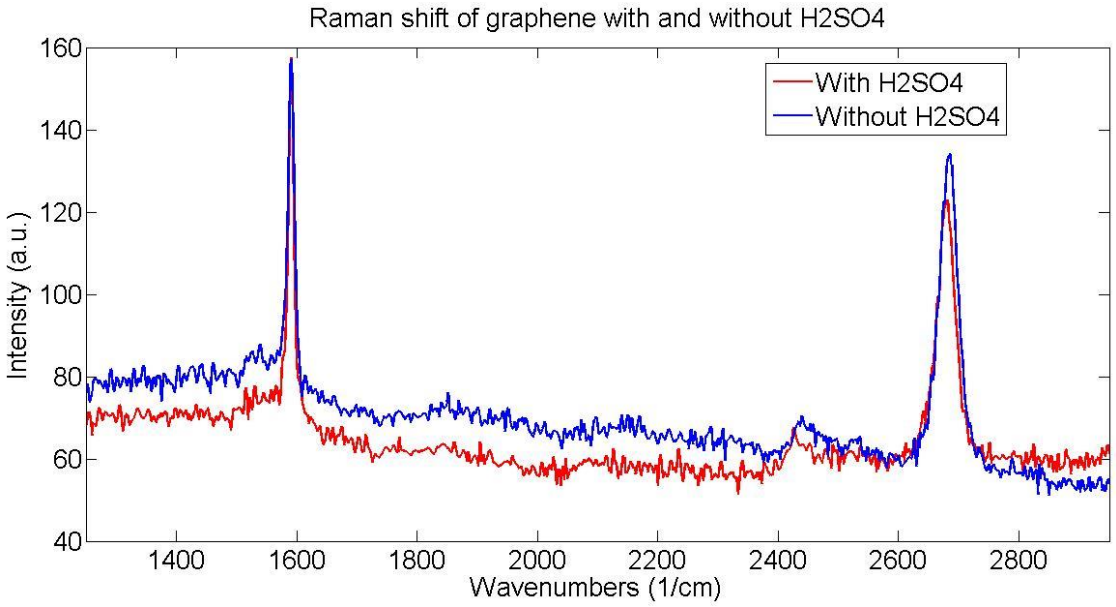

Figure 4.12 Raman shift of graphene with and without H_2SO_4.

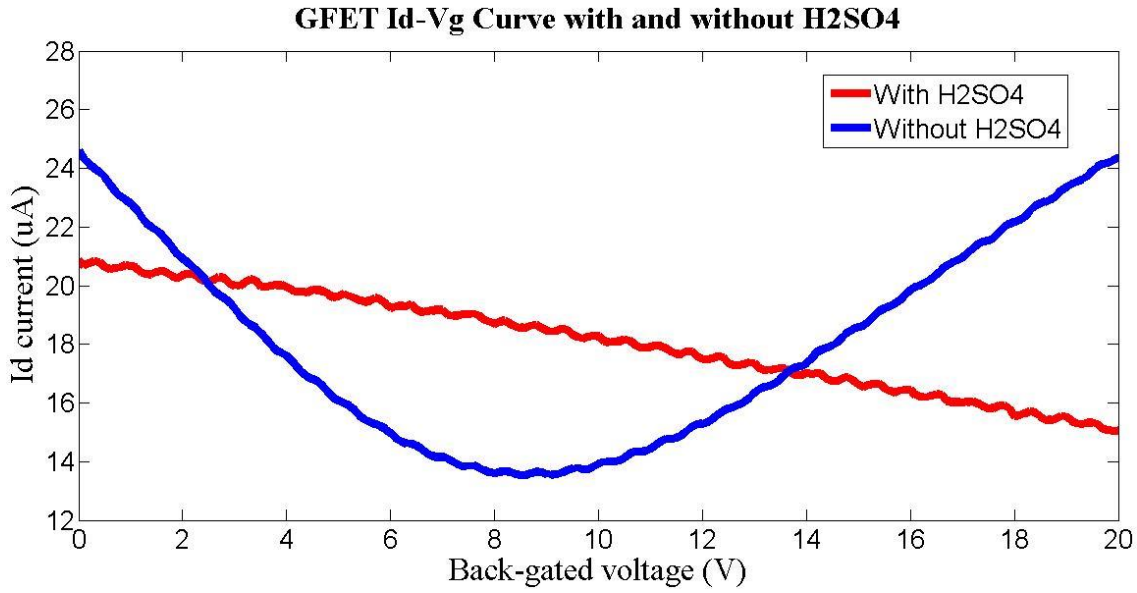

Figure 4.13 GFET Id-Vg Curve with and without H_2SO_4.

4.5 Raman spectroscopy of reversible graphene/graphene oxide device

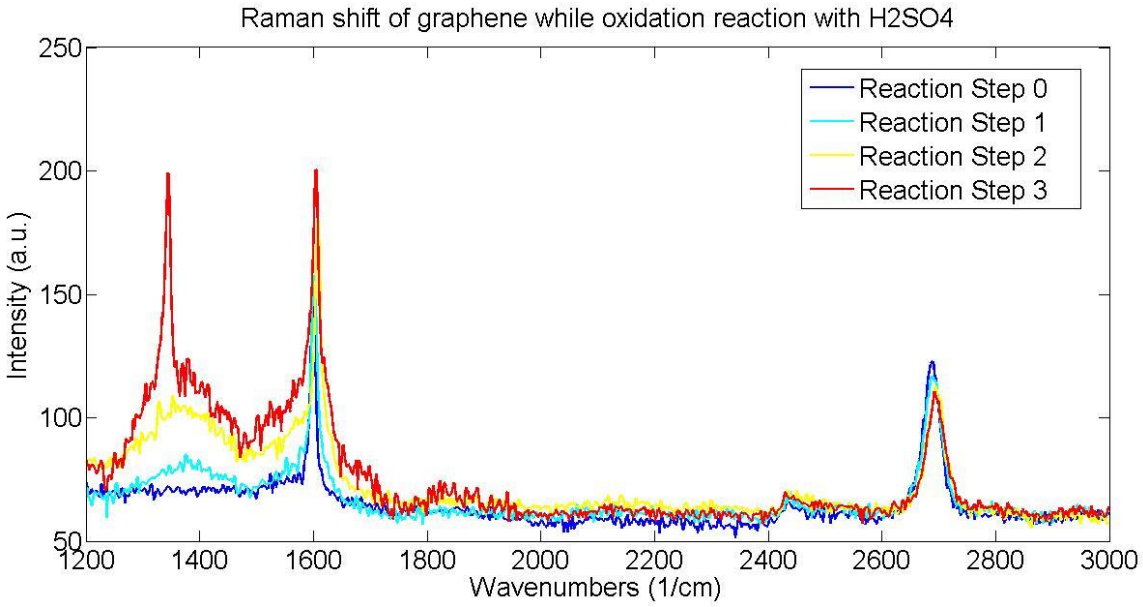

Figure 4.14 Raman shift of graphene while oxidation reaction with H_2SO_4.

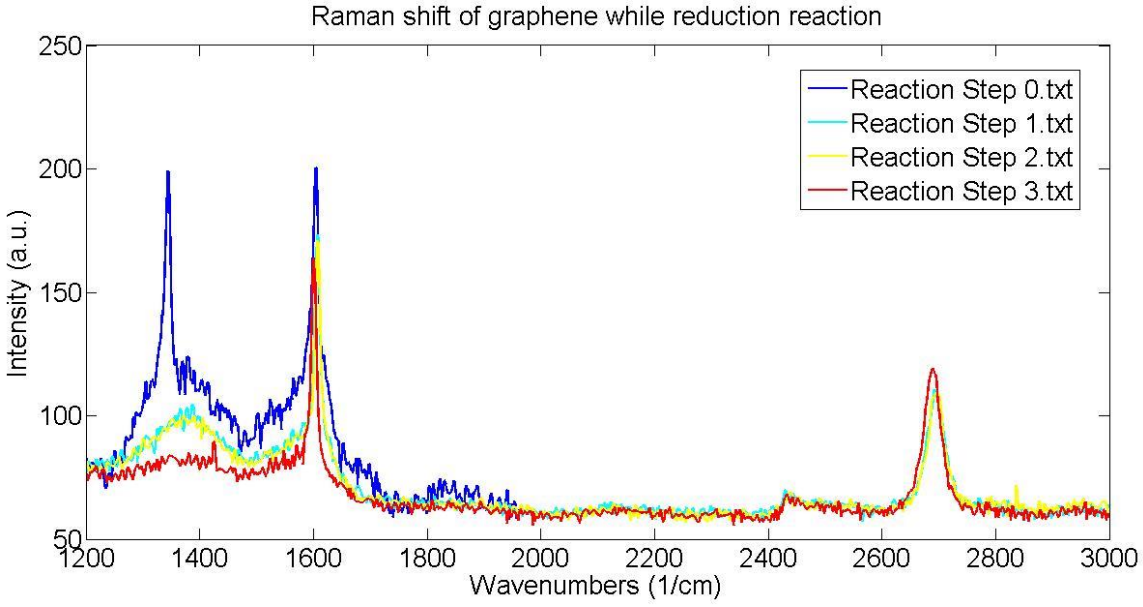

Figure 4.15 Raman shift of graphene while reduction reaction.

5. References

1 Eda, G., Mattevi, C., Yamaguchi, H., Kim, H. & Chhowalla, M. Insulator to Semimetal Transition in Graphene Oxide. *The Journal of Physical Chemistry C* **113**, 15768-15771, doi:10.1021/jp9051402 (2009).

2 Loh, K. P., Bao, Q., Eda, G. & Chhowalla, M. Graphene oxide as a chemically tunable platform for optical applications. *Nat Chem* **2**, 1015-1024 (2010).

3 Zhou, Y., Bao, Q., Tang, L. A. L., Zhong, Y. & Loh, K. P. Hydrothermal Dehydration for the "Green" Reduction of Exfoliated Graphene Oxide to Graphene and Demonstration of Tunable Optical Limiting Properties. *Chemistry of Materials* **21**, 2950-2956, doi:10.1021/cm9006603 (2009).

4 Kozawa, D., Miyauchi, Y., Mouri, S. & Matsuda, K. Exploring the Origin of Blue and Ultraviolet Fluorescence in Graphene Oxide. *The Journal of Physical Chemistry Letters* **4**, 2035-2040, doi:10.1021/jz400930f (2013).

5 Cushing, S. K., Li, M., Huang, F. & Wu, N. Origin of Strong Excitation Wavelength Dependent Fluorescence of Graphene Oxide. *ACS Nano* **8**, 1002-1013, doi:10.1021/nn405843d (2014).

6 Andreoni, W. *The physics of fullerene-based and fullerene-related materials*. Vol. 23 (Springer Science & Business Media, 2000).

7 中西毅. R. Saito, G. Dresselhaus and MS Dresselhaus, Physical Properties of Carbon Nanotubes, Imperial College Press, London, 1998, xii+ 259p., 22× 15.5 cm,\ 10,560 [学部・大学院向, 専門書]. *日本物理學會誌* **54**, 832-833 (1999).

8 Geim, A. K. & Novoselov, K. S. The rise of graphene. *Nat Mater* **6**, 183-191 (2007).

9 Schaller, R. R. Moore's law: past, present and future. *Spectrum, IEEE* **34**, 52-59, doi:10.1109/6.591665 (1997).

10 Castro Neto, A. H., Guinea, F., Peres, N. M. R., Novoselov, K. S. & Geim, A. K. The electronic properties of graphene. *Reviews of Modern Physics* **81**, 109-162 (2009).

11 Peres, N. The transport properties of graphene. *Journal of physics. Condensed matter: an Institute of Physics journal* **21**, 323201-323201 (2009).

12 Freitag, M. Graphene: nanoelectronics goes flat out. *Nature nanotechnology* **3**, 455-457 (2008).

13 Ashcroft, N. & Mermin, N. Solid State Physics (Brooks Cole, 1976). *Cited on*, 45.

14 Chen, Z. & Appenzeller, J. in *Electron Devices Meeting, 2008. IEDM 2008. IEEE International.* 1-4 (IEEE).

15 Adam, S., Hwang, E., Galitski, V. & Sarma, S. D. A self-consistent theory for graphene transport. *Proceedings of the National Academy of Sciences* **104**, 18392-18397 (2007).

16 Hwang, E. & Sarma, S. D. Acoustic phonon scattering limited carrier mobility in two-dimensional extrinsic graphene. *Physical Review B* **77**, 115449 (2008).

17 Stauber, T., Peres, N. & Guinea, F. Electronic transport in graphene: A semiclassical approach including midgap states. *Physical Review B* **76**, 205423 (2007).

18 Chen, J.-H., Jang, C., Xiao, S., Ishigami, M. & Fuhrer, M. S. Intrinsic and extrinsic performance limits of graphene devices on SiO2. *Nature nanotechnology* **3**, 206-209 (2008).

19 Du, X., Skachko, I., Duerr, F., Luican, A. & Andrei, E. Y. Fractional quantum Hall effect and insulating phase of Dirac electrons in graphene. *Nature* **462**, 192-195 (2009).

20 Bolotin, K., Sikes, K., Hone, J., Stormer, H. & Kim, P. Temperature-dependent transport in suspended graphene. *Physical review letters* **101**, 096802 (2008).

21 Rumyantsev, S., Liu, G., Potyrailo, R. A., Balandin, A. A. & Shur, M. S. Selective sensing of individual gases using graphene devices. *Sensors Journal, IEEE* **13**, 2818-2822 (2013).

22 Rumyantsev, S., Liu, G., Stillman, W., Shur, M. & Balandin, A. Electrical and noise characteristics of graphene field-effect transistors: ambient effects, noise sources and physical mechanisms. *Journal of Physics: Condensed Matter* **22**, 395302 (2010).

23 Schedin, F. *et al.* Detection of individual gas molecules adsorbed on graphene. *Nature materials* **6**, 652-655 (2007).

24 Iyechika, Y. Application of graphene to high-speed transistors: expectations and challenges. *Sci. Technol. Trends* **37**, 76-92 (2010).

25 Balog, R. *et al.* Bandgap opening in graphene induced by patterned hydrogen adsorption. *Nat Mater* **9**, 315-319, doi:http://www.nature.com/nmat/journal/v9/n4/abs/nmat2710.html#supplementary-information (2010).

26 Novoselov, K. S. *et al.* Two-dimensional gas of massless Dirac fermions in graphene. *Nature* **438**, 197-200 (2005).

27 Baringhaus, J. *et al.* Exceptional ballistic transport in epitaxial graphene nanoribbons. *Nature* **506**, 349-354, doi:10.1038/nature12952

http://www.nature.com/nature/journal/v506/n7488/abs/nature12952.html#supplementary-information (2014).

28 Zhang, Y., Tan, Y.-W., Stormer, H. L. & Kim, P. Experimental observation of the quantum Hall effect and Berry's phase in graphene. *Nature* **438**, 201-204, doi:http://www.nature.com/nature/journal/v438/n7065/suppinfo/nature04235_S1.html (2005).

29 Jung, I., Dikin, D. A., Piner, R. D. & Ruoff, R. S. Tunable Electrical Conductivity of Individual Graphene Oxide Sheets Reduced at "Low" Temperatures. *Nano letters* **8**, 4283-4287, doi:10.1021/nl8019938 (2008).

30 Fowler, J. D. *et al.* Practical Chemical Sensors from Chemically Derived Graphene. *ACS Nano* **3**, 301-306, doi:10.1021/nn800593m (2009).

31 Chitara, B., Panchakarla, L. S., Krupanidhi, S. B. & Rao, C. N. R. Infrared Photodetectors Based on Reduced Graphene Oxide and Graphene Nanoribbons. *Advanced materials* **23**, 5419-5424, doi:10.1002/adma.201101414 (2011).

32 Ghosh, S., Sarker, B. K., Chunder, A., Zhai, L. & Khondaker, S. I. Position dependent photodetector from large area reduced graphene oxide thin films. *Applied Physics Letters* **96**, 163109, doi:doi:http://dx.doi.org/10.1063/1.3415499 (2010).

33 Zhan, Z., Zheng, L., Pan, Y., Sun, G. & Li, L. Self-powered, visible-light photodetector based on thermally reduced graphene oxide-ZnO (rGO-ZnO) hybrid nanostructure. *Journal of Materials Chemistry* **22**, 2589-2595, doi:10.1039/C1JM13920G (2012).

34 Liu, Y., Dong, X. & Chen, P. Biological and chemical sensors based on graphene materials. *Chemical Society reviews* **41**, 2283-2307, doi:10.1039/C1CS15270J (2012).

35 Gadipelli, S. *et al.* A highly practical route for large-area, single layer graphene from liquid carbon sources such as benzene and methanol. *Journal of Materials Chemistry* **21**, 16057-16065, doi:10.1039/C1JM12938D (2011).

36 Mattevi, C., Kim, H. & Chhowalla, M. A review of chemical vapour deposition of graphene on copper. *Journal of Materials Chemistry* **21**, 3324-3334, doi:10.1039/C0JM02126A (2011).

37 Chavez, K. & Hess, D. A novel method of etching copper oxide using acetic acid. *Journal of The Electrochemical Society* **148**, G640-G643 (2001).

38 Liu, W., Li, H., Xu, C., Khatami, Y. & Banerjee, K. Synthesis of high-quality monolayer and bilayer graphene on copper using chemical vapor deposition. *Carbon* **49**, 4122-4130 (2011).

39 Butt, M. Effect of hydrogen attack on the strength of high purity copper. *Journal of Materials Science Letters* **2**, 1-2 (1983).

40 Kim, H. *et al.* Activation Energy Paths for Graphene Nucleation and Growth on Cu. *ACS Nano* **6**, 3614-3623, doi:10.1021/nn3008965 (2012).

41 Yu, Q. *et al.* Control and characterization of individual grains and grain boundaries in graphene grown by chemical vapour deposition. *Nat Mater* **10**, 443-449, doi:http://www.nature.com/nmat/journal/v10/n6/abs/nmat3010.html#supplementary-information (2011).

42 Zhang, Y., Zhang, L. & Zhou, C. Review of Chemical Vapor Deposition of Graphene and Related Applications. *Accounts of Chemical Research* **46**, 2329-2339, doi:10.1021/ar300203n (2013).

43 Li, X. *et al.* Large-Area Synthesis of High-Quality and Uniform Graphene Films on Copper Foils. *Science* **324**, 1312-1314, doi:10.1126/science.1171245 (2009).

44 Ferrari, A. C. & Basko, D. M. Raman spectroscopy as a versatile tool for studying the properties of graphene. *Nat Nano* **8**, 235-246, doi:http://www.nature.com/nnano/journal/v8/n4/abs/nnano.2013.46.html#supplementary-information (2013).

45 Ferrari, A. C. *et al.* Raman Spectrum of Graphene and Graphene Layers. *Physical Review Letters* **97**, 187401 (2006).

46 Li, X. *et al.* Graphene films with large domain size by a two-step chemical vapor deposition process. *Nano letters* **10**, 4328-4334 (2010).

47 Gao, L. *et al.* Repeated growth and bubbling transfer of graphene with millimetre-size single-crystal grains using platinum. *Nature communications* **3**, 699 (2012).

48 Li, X. *et al.* Large-area graphene single crystals grown by low-pressure chemical vapor deposition of methane on copper. *Journal of the American Chemical Society* **133**, 2816-2819 (2011).

49 Wang, Y. *et al.* Electrochemical delamination of CVD-grown graphene film: toward the recyclable use of copper catalyst. *ACS nano* **5**, 9927-9933 (2011).